C1

A B

EUROPEAN ORGANIZATION FOR NUCLEAR RESEARCH

CERN-PPE/93-221
16 December 1993

SW 9405

CERN LIBRARIES, GENEVA

P00020751

An investigation of B_d^0 and B_s^0 oscillation

The ALEPH Collaboration*

Abstract

$B^0\overline{B}^0$ oscillation is studied using almost a million hadronic Z decays collected by the ALEPH experiment at LEP. Events are selected with two leptons present, on opposite sides of the event and with high transverse momentum. The leptons are expected to be dominantly from b decays; a topological vertexing technique is applied to measure the decay length of the b hadrons, and their momentum is determined using an energy-flow method. The fraction of events in which the leptons have the same charge is studied as a function of the measured decay time, and clear evidence is seen for the time-dependent nature of $B_d^0\overline{B}_d^0$ mixing. The frequency measured for the oscillation corresponds to a mass difference for the B_d^0 mass eigenstates $\Delta m_d = (3.3\ ^{+0.5}_{-0.4} \pm 0.7) \times 10^{-4}\,\mathrm{eV}/c^2$. Allowing a second frequency component for the B_s^0 a high value for Δm_s is favoured, leading to the limit $\Delta m_s > 12 \times 10^{-4}\,\mathrm{eV}/c^2$ (95 % CL), from which $(\Delta m/\Gamma)_s > 2.0$ is derived.

(Submitted to Phys. Lett. B)

*See the following pages for the list of authors.

The ALEPH Collaboration

D. Buskulic, I. De Bonis, D. Decamp, P. Ghez, C. Goy, J.-P. Lees, M.-N. Minard, P. Odier, B. Pietrzyk
Laboratoire de Physique des Particules (LAPP), IN^2P^3-CNRS, 74019 Annecy-le-Vieux Cedex, France

F. Ariztizabal, P. Comas, J.M. Crespo, I. Efthymiopoulos, E. Fernandez, M. Fernandez-Bosman, V. Gaitan, Ll. Garrido,[29] M. Martinez, T. Mattison,[30] S. Orteu, A. Pacheco, C. Padilla, A. Pascual
Institut de Fisica d'Altes Energies, Universitat Autonoma de Barcelona, 08193 Bellaterra (Barcelona), Spain[7]

D. Creanza, M. de Palma, A. Farilla, G. Iaselli, G. Maggi, N. Marinelli, S. Natali, S. Nuzzo, A. Ranieri, G. Raso, F. Romano, F. Ruggieri, G. Selvaggi, L. Silvestris, P. Tempesta, G. Zito
Dipartimento di Fisica, INFN Sezione di Bari, 70126 Bari, Italy

Y. Chai, H. Hu, D. Huang, X. Huang, J. Lin, T. Wang, Y. Xie, D. Xu, R. Xu, J. Zhang, L. Zhang, W. Zhao
Institute of High-Energy Physics, Academia Sinica, Beijing, The People's Republic of China[8]

G. Bonvicini, J. Boudreau, D. Casper, H. Drevermann, R.W. Forty, G. Ganis, C. Gay, M. Girone, R. Hagelberg, J. Harvey, J. Hilgart,[27] R. Jacobsen, B. Jost, J. Knobloch, I. Lehraus, M. Maggi, C. Markou, P. Mato, H. Meinhard, A. Minten, R. Miquel, H.-G. Moser, P. Palazzi, J.R. Pater, J.A. Perlas, P. Perrodo, J.-F. Pusztaszeri, F. Ranjard, L. Rolandi, J. Rothberg,[2] T. Ruan, M. Saich, D. Schlatter, M. Schmelling, F. Sefkow,[6] W. Tejessy, I.R. Tomalin, R. Veenhof, H. Wachsmuth, S. Wasserbaech,[2] W. Wiedenmann, T. Wildish, W. Witzeling, J. Wotschack
European Laboratory for Particle Physics (CERN), 1211 Geneva 23, Switzerland

Z. Ajaltouni, M. Bardadin-Otwinowska, A. Barres, C. Boyer, A. Falvard, P. Gay, C. Guicheney, P. Henrard, J. Jousset, B. Michel, J-C. Montret, D. Pallin, P. Perret, F. Podlyski, J. Proriol, F. Saadi
Laboratoire de Physique Corpusculaire, Université Blaise Pascal, IN^2P^3-CNRS, Clermont-Ferrand, 63177 Aubière, France

T. Fearnley, J.B. Hansen, J.D. Hansen, J.R. Hansen, P.H. Hansen, S.D. Johnson, R. Møllerud, B.S. Nilsson[1]
Niels Bohr Institute, 2100 Copenhagen, Denmark[9]

A. Kyriakis, E. Simopoulou, I. Siotis, A. Vayaki, K. Zachariadou
Nuclear Research Center Demokritos (NRCD), Athens, Greece

J. Badier, A. Blondel, G. Bonneaud, J.C. Brient, P. Bourdon, G. Fouque, L. Passalacqua, A. Rougé, M. Rumpf, R. Tanaka, M. Verderi, H. Videau
Laboratoire de Physique Nucléaire et des Hautes Energies, Ecole Polytechnique, IN^2P^3-CNRS, 91128 Palaiseau Cedex, France

D.J. Candlin, M.I. Parsons, E. Veitch
Department of Physics, University of Edinburgh, Edinburgh EH9 3JZ, United Kingdom[10]

E. Focardi, L. Moneta, G. Parrini
Dipartimento di Fisica, Università di Firenze, INFN Sezione di Firenze, 50125 Firenze, Italy

M. Corden, M. Delfino,[12] C. Georgiopoulos, D.E. Jaffe, D. Levinthal[15]
Supercomputer Computations Research Institute, Florida State University, Tallahassee, FL 32306-4052, USA [13,14]

A. Antonelli, G. Bencivenni, G. Bologna,[4] F. Bossi, P. Campana, G. Capon, F. Cerutti, V. Chiarella, G. Felici, P. Laurelli, G. Mannocchi,[5] F. Murtas, G.P. Murtas, M. Pepe-Altarelli, S. Salomone
Laboratori Nazionali dell'INFN (LNF-INFN), 00044 Frascati, Italy

P. Colrain, I. ten Have, I.G. Knowles, J.G. Lynch, W. Maitland, W.T. Morton, C. Raine, P. Reeves, J.M. Scarr, K. Smith, M.G. Smith, A.S. Thompson, S. Thorn, R.M. Turnbull

Department of Physics and Astronomy, University of Glasgow, Glasgow G12 8QQ, United Kingdom[10]

B. Brandl, O. Braun, C. Geweniger, P. Hanke, V. Hepp, E.E. Kluge, Y. Maumary, A. Putzer,[1] B. Rensch, A. Stahl, K. Tittel, M. Wunsch

Institut für Hochenergiephysik, Universität Heidelberg, 69120 Heidelberg, Fed. Rep. of Germany[16]

R. Beuselinck, D.M. Binnie, W. Cameron, M. Cattaneo, D.J. Colling, P.J. Dornan, J.F. Hassard, N.M. Lieske,[25] A. Moutoussi, J. Nash, S. Patton, D.G. Payne, M.J. Phillips, G. San Martin, J.K. Sedgbeer, A.G. Wright

Department of Physics, Imperial College, London SW7 2BZ, United Kingdom[10]

P. Girtler, D. Kuhn, G. Rudolph, R. Vogl

Institut für Experimentalphysik, Universität Innsbruck, 6020 Innsbruck, Austria[18]

C.K. Bowdery, T.J. Brodbeck, A.J. Finch, F. Foster, G. Hughes, D. Jackson, N.R. Keemer, M. Nuttall, A. Patel, T. Sloan, S.W. Snow, E.P. Whelan

Department of Physics, University of Lancaster, Lancaster LA1 4YB, United Kingdom[10]

A. Galla, A.M. Greene, K. Kleinknecht, J. Raab, B. Renk, H.-G. Sander, H. Schmidt, S.M. Walther, R. Wanke, B. Wolf

Institut für Physik, Universität Mainz, 55099 Mainz, Fed. Rep. of Germany[16]

A.M. Bencheikh, C. Benchouk, A. Bonissent, D. Calvet, J. Carr, P. Coyle, C. Diaconu, J. Drinkard,[3] F. Etienne, D. Nicod, P. Payre, L. Roos, D. Rousseau, P. Schwemling, M. Talby

Centre de Physique des Particules, Faculté des Sciences de Luminy, IN^2P^3-CNRS, 13288 Marseille, France

S. Adlung, R. Assmann, C. Bauer, W. Blum, D. Brown, P. Cattaneo,[23] B. Dehning, H. Dietl, F. Dydak,[21] M. Frank, A.W. Halley, K. Jakobs, J. Lauber, G. Lütjens, G. Lutz, W. Männer, R. Richter, J. Schröder, A.S. Schwarz, R. Settles, H. Seywerd, U. Stierlin, U. Stiegler, R. St. Denis, G. Wolf

Max-Planck-Institut für Physik, Werner-Heisenberg-Institut, 80805 München, Fed. Rep. of Germany[16]

R. Alemany, J. Boucrot,[1] O. Callot, A. Cordier, M. Davier, L. Duflot, J.-F. Grivaz, Ph. Heusse, P. Janot, D.W. Kim,[19] F. Le Diberder, J. Lefrançois, A.-M. Lutz, G. Musolino, M.-H. Schune, J.-J. Veillet, I. Videau

Laboratoire de l'Accélérateur Linéaire, Université de Paris-Sud, IN^2P^3-CNRS, 91405 Orsay Cedex, France

D. Abbaneo, G. Bagliesi, G. Batignani, U. Bottigli, C. Bozzi, G. Calderini, M. Carpinelli, M.A. Ciocci, V. Ciulli, R. Dell'Orso, I. Ferrante, F. Fidecaro, L. Foà, F. Forti, A. Giassi, M.A. Giorgi, A. Gregorio, F. Ligabue, A. Lusiani, E.B. Mannelli, P.S. Marrocchesi, A. Messineo, F. Palla, G. Rizzo, G. Sanguinetti, P. Spagnolo, J. Steinberger, R. Tenchini,[1] G. Tonelli,[28] G. Triggiani, A. Valassi, C. Vannini, A. Venturi, P.G. Verdini, J. Walsh

Dipartimento di Fisica dell'Università, INFN Sezione di Pisa, e Scuola Normale Superiore, 56010 Pisa, Italy

A.P. Betteridge, Y. Gao, M.G. Green, D.L. Johnson, P.V. March, T. Medcalf, Ll.M. Mir, I.S. Quazi, J.A. Strong

Department of Physics, Royal Holloway & Bedford New College, University of London, Surrey TW20 OEX, United Kingdom[10]

V. Bertin, D.R. Botterill, R.W. Clifft, T.R. Edgecock, S. Haywood, M. Edwards, P.R. Norton, J.C. Thompson

Particle Physics Dept., Rutherford Appleton Laboratory, Chilton, Didcot, Oxon OX11 OQX, United Kingdom[10]

B. Bloch-Devaux, P. Colas, H. Duarte, S. Emery, W. Kozanecki, E. Lançon, M.C. Lemaire, E. Locci, B. Marx, P. Perez, J. Rander, J.-F. Renardy, A. Rosowsky, A. Roussarie, J.-P. Schuller, J. Schwindling, D. Si Mohand, B. Vallage

Service de Physique des Particules, DAPNIA, CE-Saclay, 91191 Gif-sur-Yvette Cedex, France[17]

R.P. Johnson, A.M. Litke, G. Taylor, J. Wear

Institute for Particle Physics, University of California at Santa Cruz, Santa Cruz, CA 95064, USA[22]

W. Babbage, C.N. Booth, C. Buttar, S. Cartwright, F. Combley, I. Dawson, L.F. Thompson

Department of Physics, University of Sheffield, Sheffield S3 7RH, United Kingdom[10]

E. Barberio,[31] A. Böhrer, S. Brandt, G. Cowan,[1] C. Grupen, G. Lutters, F. Rivera,[26] U. Schäfer, L. Smolik

Fachbereich Physik, Universität Siegen, 57068 Siegen, Fed. Rep. of Germany[16]

L. Bosisio, R. Della Marina, G. Giannini, B. Gobbo, L. Pitis, F. Ragusa[20]

Dipartimento di Fisica, Università di Trieste e INFN Sezione di Trieste, 34127 Trieste, Italy

L. Bellantoni, W. Chen, J.S. Conway,[24] Z. Feng, D.P.S. Ferguson, Y.S. Gao, J. Grahl, J.L. Harton, O.J. Hayes III, J.M. Nachtman, Y.B. Pan, Y. Saadi, M. Schmitt, I. Scott, V. Sharma, Z.H. Shi, J.D. Turk, A.M. Walsh, F.V. Weber, Sau Lan Wu, X. Wu, M. Zheng, G. Zobernig

Department of Physics, University of Wisconsin, Madison, WI 53706, USA[11]

---

[1] Now at CERN, PPE Division, 1211 Geneva 23, Switzerland.
[2] Permanent address: University of Washington, Seattle, WA 98195, USA.
[3] Now at University of California, Irvine, CA 92717, USA.
[4] Also Istituto di Fisica Generale, Università di Torino, Torino, Italy.
[5] Also Istituto di Cosmo-Geofisica del C.N.R., Torino, Italy.
[6] Now at DESY, Hamburg, Germany.
[7] Supported by CICYT, Spain.
[8] Supported by the National Science Foundation of China.
[9] Supported by the Danish Natural Science Research Council.
[10] Supported by the UK Science and Engineering Research Council.
[11] Supported by the US Department of Energy, contract DE-AC02-76ER00881.
[12] On leave from Universitat Autonoma de Barcelona, Barcelona, Spain.
[13] Supported by the US Department of Energy, contract DE-FG05-92ER40742.
[14] Supported by the US Department of Energy, contract DE-FC05-85ER250000.
[15] Present address: Lion Valley Vineyards, Cornelius, Oregon, U.S.A.
[16] Supported by the Bundesministerium für Forschung und Technologie, Fed. Rep. of Germany.
[17] Supported by the Direction des Sciences de la Matière, C.E.A.
[18] Supported by Fonds zur Förderung der wissenschaftlichen Forschung, Austria.
[19] Permanent address: Kangnung National University, Kangnung, Korea.
[20] Now at Dipartimento di Fisica, Università di Milano, Milano, Italy.
[21] Also at CERN, PPE Division, 1211 Geneva 23, Switzerland.
[22] Supported by the US Department of Energy, grant DE-FG03-92ER40689.
[23] Now at Università di Pavia, Pavia, Italy.
[24] Now at Rutgers University, Piscataway, NJ 08854, USA.
[25] Now at Oxford University, Oxford OX1 3RH, U.K.
[26] Partially supported by Colciencias, Colombia.
[27] Now at SSCL, Dallas 75237-3946, TX, U.S.A.
[28] Also at Istituto di Matematica e Fisica, Università di Sassari, Sassari, Italy.
[29] Permanent address: Dept. d'Estructura i Constituens de la Materia, Universitat de Barcelona, 08208 Barcelona, Spain.
[30] Now at SLAC, Stanford, CA 94309, U.S.A.
[31] Now at Università della Calabria, Cosenza, Italy.

1 Introduction

The phenomenon of $B^0\overline{B}^0$ mixing is well established [1]. The observed B^0 particle or anti-particle states are linear combinations of the states with well defined mass. Their difference in mass Δm leads to a time-dependent phase difference between their wavefunctions, and thus the probability to observe a B^0 or $\overline{B}^0$ oscillates as a function of proper time. For an initially pure B^0 state, the probability of observing the decay of a $\overline{B}^0$ is given by

$$\mathrm{Prob}(\overline{B}^0) = \frac{1-\cos(\Delta m t)}{2}\, \mathrm{e}^{-\Gamma t} , \tag{1}$$

in units $\hbar = c = 1$, where the decay widths Γ for the two states have been assumed equal and the effects of CP violation (expected to be small) have been neglected [1]. The time-integrated probability of mixing is then

$$\chi = \frac{1}{2}\frac{(\Delta m/\Gamma)^2}{1+(\Delta m/\Gamma)^2} , \tag{2}$$

where the dimensionless oscillation parameter $\Delta m/\Gamma$ has been introduced, which expresses the oscillation frequency in terms of the lifetime. This formalism applies to both the B_d^0 and B_s^0 mesons (with parameters distinguished using subscripts d and s).

In the Standard Model mixing occurs via second-order W-exchange, and the expected mass differences for the B_d^0 and B_s^0 have been calculated. They depend on the Kobayashi-Maskawa matrix elements V_{td} and V_{ts} respectively, but also on the as yet unmeasured top-quark mass, and other poorly determined hadronic factors. The ratios of such factors for the B_d^0 and B_s^0 are expected to be close to unity, however, with rather smaller uncertainty, and thus the measurement of both B_d^0 and B_s^0 mixing would constrain the matrix elements:

$$\frac{\Delta m_s}{\Delta m_d} = (1.19 \pm 0.10) \times \left|\frac{V_{ts}}{V_{td}}\right|^2 , \tag{3}$$

where the estimate of the coefficient has been taken from Reference [2]. Assuming unitarity of the Kobayashi-Maskawa matrix this ratio is already constrained by measurements of the Cabibbo angle ($\sin\theta_c = 0.221 \pm 0.002$ [3]) and $|V_{ub}/V_{cb}| = 0.08 \pm 0.03$ [4], leading to the Standard Model prediction $\Delta m_s/\Delta m_d > 8$ (95 % CL).

The time-integrated probability of mixing has been measured for the B_d^0 by experiments running at the $\Upsilon(4S)$ [5] with the result $\chi_d = 0.158 \pm 0.026$ [6], which corresponds via Equation (2) to $(\Delta m/\Gamma)_d = 0.68 \pm 0.08$. At higher energies the B_s^0 is also produced, and the probability of mixing is then a weighted average of the values for the two neutral B mesons:

$$\overline{\chi} = f_d\chi_d + f_s\chi_s , \tag{4}$$

where f_d and f_s are the fractions of b hadrons that are produced as B_d^0 and B_s^0 mesons respectively. For a given assumption of the value of these fractions ($f_d = 0.40$, $f_s = 0.12$) the measurements of $\overline{\chi}$ [7, 8] can be used to extract $\chi_s > 0.22$ (95 % CL) [6], but this only corresponds to a poor constraint on the oscillation parameter, $(\Delta m/\Gamma)_s > 0.9$. For larger values of $(\Delta m/\Gamma)_s$ the time-integrated probability of mixing χ_s quickly saturates at 0.5, and to progress further an experimental technique that exploits the time-dependence of Equation (1) is required.

For the measurement of $B^0\overline{B}^0$ mixing it is necessary to determine the particle/antiparticle state of the B^0 at both its production and decay, and this is achieved here using dilepton events in hadronic Z decays. In the decay $Z \to b\bar{b}$, the b and $\bar{b}$ quarks are produced as an oppositely charged pair; furthermore, in the semileptonic decay $b \to c\ell^-\bar{\nu}$ the charge of the lepton has the same sign as that of the quark. Thus if a semileptonic decay is observed on one side of a $b\bar{b}$ event, the sign of the lepton charge can be used to tag the production state of the b hadron on the other side. If a semileptonic decay also occurs there, then in the absence of mixing the leptons would be expected to have opposite charges. If, on the other hand, either of the b hadrons is a B^0 that undergoes mixing, then a like-signed dilepton event results. This is complicated by the presence of mistagging, mainly from cascade decays $b \to c \to \ell^+$ where the b hadron decays to a charmed particle which then decays semileptonically. Nevertheless, the study of the fraction of dilepton events in which the leptons have like sign can provide a measurement of $\overline{\chi}$, as previously reported [8].

The new development here is the addition of proper-time information for the decay of the b hadrons. This is achieved by measuring the decay length of the b hadron, using the lepton and other charged tracks in an inclusive vertexing technique. The decay distance is converted to proper time by estimating the momentum of the b hadron from the momenta of its decay products. Each dilepton event can provide up to two measurements of the decay time, and the distribution of reconstructed decay times is fitted using a maximum likelihood technique to extract the oscillation parameters. Since B^0_d and B^0_s mesons both contribute to dilepton events, the measurement is sensitive to Δm_d and Δm_s. Extracting both parameters involves searching for two separate frequency components in the decay-time distribution.

2 Event selection

The ALEPH detector has been described in detail elsewhere [9]. A high resolution vertex detector was added in 1991, consisting of two layers of double-sided silicon microstrip detectors. The inner layer is at an average radius of 6.3 cm from the beam axis, and covers 85 % of the solid angle, whilst the outer layer is at a radius of 10.8 cm and covers 69 %. The spatial resolution in the $r\phi$ and rz projections (transverse to and along the beam axis respectively) is 12 μm at normal incidence [10]. The vertex detector is surrounded by a drift chamber with eight axial wire layers up to a radius of 26 cm, and then a time projection chamber (TPC) that measures up to 21 space points per track at radii between 40 cm and 171 cm. These detectors are immersed in an axial magnetic field of 1.5 T, and together measure the momentum of charged particles with a resolution $\sigma(p)/p = 0.0006\,p$ (p in GeV). The TPC also provides up to 330 measurements of the specific ionization ($\mathrm{d}E/\mathrm{d}x$) of a track. It is surrounded by an electromagnetic calorimeter of lead/proportional-chamber construction, segmented into $0.8° \times 0.8°$ projective towers and read out in three sections in depth, with energy resolution $\sigma(E)/E = 0.18\,/\sqrt{E}$ (E in GeV). The iron return yoke of the magnet is instrumented with streamer tubes to form a hadron calorimeter, with a thickness of over 7 interaction lengths, and this is surrounded by two further double-layers of streamer tubes to aid muon identification.

The data recorded in 1991 and 1992 are used, with centre-of-mass energy at and near the Z mass. 977,000 hadronic events are selected, as described in Reference [11]. Leptons, here referring to electrons and muons, are then identified. The candidate lepton track is required to have at least 5 TPC hits, polar angle θ satisfying $|\cos\theta| < 0.95$, and to pass within 5 mm of the beam axis. For electrons the momentum is required to be greater than 2 GeV, and identification is performed using the shower shape in the electromagnetic calorimeter and $\mathrm{d}E/\mathrm{d}x$ information from the TPC [12]. If any other oppositely-charged track passes within 1 cm in space of the electron candidate and forms an invariant mass with it of less than 20 MeV, then the candidate is rejected as a possible photon conversion. For muons the momentum is required to be greater than 3 GeV. Candidates are selected that have a pattern of digital hits in the hadron calorimeter consistent with the passage of a muon [12], and the track is required to have at least one associated muon chamber hit.

Jets are reconstructed in each event using charged and neutral particles (determined with an energy-flow algorithm [13]) that are clustered using the scaled-invariant-mass technique [14], with clustering parameter $y_{cut} = (6\,\mathrm{GeV}/E_{cm})^2$. At least two leptons are required to be present in the event, each with momentum less than 90 % of the total energy of the jet to which it belongs; 22,000 such dilepton events are selected. The transverse momentum p_T of the lepton is calculated relative to the jet axis after first removing the lepton from the jet [12], and both leptons are required to satisfy $p_T > 1.25\,\mathrm{GeV}$. They must also be associated to different jets, with the two jets in opposite hemispheres (where the hemispheres are defined using the thrust axis, calculated using charged and neutral particles); this leaves 1863 events. The proper times of the candidate b decays are then measured, as described in the following section. To qualify for decay-time measurement, the lepton track is required to have at least one vertex detector hit in both the $r\phi$ and rz projections. At least one other decay track must be found, making a good vertex with the lepton, as described below. Of the 1577 remaining dilepton events with at least one decay-time measurement, 902 have decay times measured on both sides, giving a total of 2479 leptons with decay-time measurement.

A sample of 1,380,000 simulated hadronic events have also been analysed. The Monte Carlo generator is based on JETSET 7.3 [15], with updated branching ratios and using the Körner-Schuler model [16] for semileptonic b decays. After applying the cuts described above for the data, 2540 dilepton events are selected, with 3654 of the leptons having a measurement of decay-time. The composition of this sample is shown in Table 1. As can be seen, the sample originates almost entirely from $b\bar{b}$ events. The 'misid' contributions refer to non-leptonic tracks which have been misidentified as leptons, and the 'decay' leptons are of non-prompt origin, from photon conversion or from kaon or pion decays in flight.

3 Decay-time reconstruction

The proper time of a b hadron decay is given by

$$t = \frac{1}{\gamma\beta}\, d \;= \frac{m_b}{p_b}\, d\,, \tag{5}$$

Number	Source	Symbol	Fraction
3178	$b \to \ell$	b	0.896
44	$b \to \tau \to \ell$		
51	$b \to J/\psi \to \ell$		
262	$b \to c \to \ell$	bc	0.075
14	$b \to \bar{c} \to \ell$		
19	$c \to \ell$	c	0.005
74	$b\bar{b}$ misid	bkg	0.024
7	$b\bar{b}$ decay		
5	$c\bar{c}$ misid		

Table 1: Composition of the lepton candidates with measured decay time in the Monte Carlo dilepton sample, classified according to their decay-time dependence (as discussed in Section 4).

where γ and β are the boost and velocity of the b hadron, and d is the decay length. The technique used to measure the decay length relies on the expectation that, apart from the leptons, most tracks in the event should originate either from the primary vertex or from the charmed particle decays. Thus after finding the primary vertex, the charmed particle decay vertex is reconstructed on each side of the event, and finally the inferred charm track is vertexed with the lepton to give the b decay point. This is illustrated in Figure 1. First the beam spot position and size are determined in the $r\phi$ projection using a common fit to the parameters of all the charged tracks in groups of 75 sequential hadronic events. The precision on the horizontal and vertical coordinates (x, y) of the beam spot is about $30\,\mu$m and $10\,\mu$m respectively; the typical *rms* spot size was $(150 \times 10)\,\mu$m in 1991, reduced by about 25 % on average in 1992 due to changes in the operation of the LEP machine. Events with two leptons are then selected as described in the previous section, and for each event all of the charged tracks (except for the two leptons) are used in a search for a primary vertex and two decay vertices.

For the primary vertex, tracks passing within 3 mm of the beam axis are used to find a coarse z vertex coordinate. Tracks passing within 3 mm in space of this point on the beam axis are extrapolated to the plane defined by the y coordinate of the beam. The χ^2 of candidate primary vertices spaced $20\,\mu$m apart on a square grid in this plane are then calculated using the track impact points and errors, with tracks used in the χ^2 calculation only if they are less than three standard deviations away from the candidate vertex. The beam position and size in x are also included in the χ^2. The grid point with minimum χ^2 is found, and the fit of a paraboloid surface to the surrounding region is used to interpolate between the grid points; the curvature of the surface gives the vertex error. The *rms* resolution of this technique is found to be about $50\,\mu$m in simulated light-quark (uds) events (in both x and z coordinates), whilst in b events the lower number and momentum of primary tracks, as well as the inadvertant inclusion of decay tracks, degrades the resolution to about $90\,\mu$m.

For each of the jets that contain a lepton, the charged tracks associated to the jet (ex-

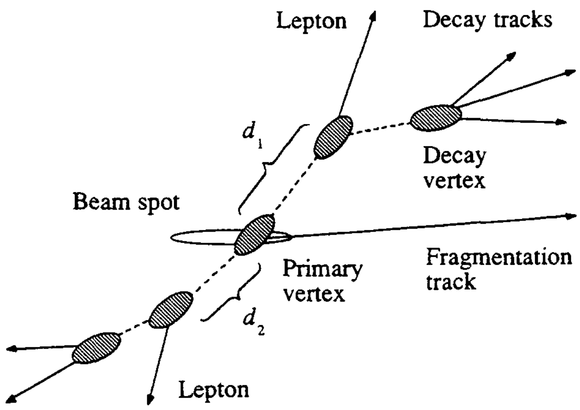

Figure 1: Schematic illustration of the decay length measurement. The shaded ellipses represent reconstructed vertices, the solid lines represent charged tracks, and the dashed lines are the tracks inferred from the reconstruction; distances d_1 and d_2 are the reconstructed b hadron decay lengths.

cluding the lepton) are then used in the search for a decay vertex. This is achieved by determining the difference in χ^2 between assigning all tracks to the primary vertex or allowing some to originate from a second vertex. The difference in χ^2 is calculated for candidate decay vertices at points on a grid, in a similar fashion as for the primary vertex, performed in two orthogonal projections containing the jet axis. The point in space which maximises the difference in χ^2 is then determined, after interpolating with a local paraboloid as for the primary vertex. A vertex is formed using tracks that pass within three standard deviations of this point. The sum of their momenta is used to define the direction of the inferred 'charm' track, constructed so that it passes through the decay vertex. If only one such track is found (which occurs in 11 % of the cases) that track is taken as the charm candidate. The charm track is finally vertexed with the lepton, to give the b decay point. Due to the inclusive nature of this technique there is the possibility of including wrong tracks in the reconstruction of the charmed particle, and a cut of $\chi^2 < 25$ is applied to the b decay vertex to reduce the effect of such misassignments whilst maintaining a high efficiency. The b decay length is taken as the separation in three dimensions of the primary and secondary vertices, projected onto the jet axis. This provides a sign for the decay length; negative values can occur due to the finite resolution.

The decay-length resolution for Monte Carlo b events is shown in Figure 2(a). It is parametrized using the sum of three Gaussians, with widths (0.23, 0.57, 2.3) mm, and fractions (0.35, 0.44, 0.21) respectively. The tails include contributions from decays in which a primary vertex track has been included in the decay vertex calculation despite the χ^2 cut, leading to some asymmetry of the tails. The mean of the distribution is -0.14 mm, and to avoid bias the reconstructed decay length is adjusted by this offset.

The decay-length resolution can be checked with real data, using events which are selected from one side of the event as being unlikely to have a significant decay length, and then measuring the apparent decay length on the other side. The selection is performed by requiring that the difference in χ^2 of the search for a decay vertex on one side of the event (as described above) is less than 4. In Monte Carlo events this selects a sample that is of 80 % *uds* composition. A fake lepton is required to be present on the other side of the event; this is a charged track that passes the selection criteria for lepton candidates, in particular the p and p_T cuts, but fails the lepton identification. The reconstructed decay-length distribution for the fake lepton is shown as the points in Figure 2 (b). The distribution is similar to that found for the Monte Carlo dileptons; it need not be identical, due to potential differences in the vertexing of *uds* and b events (such as differences in multiplicity). It can, however, be used to calibrate the dilepton resolution, by performing the same analysis with Monte Carlo fake leptons. This leads to the histogram superimposed on Figure 2 (b). A scale factor for the width of the data resolution function relative to that of the Monte Carlo is determined from a fit to the negative side of these distributions, giving a value of 1.10, and this is applied to the dilepton decay-length resolution for the data.

To convert the decay length into proper time, the 'boost term' multiplying d in Equation (5) must be determined. This is achieved by estimating the b hadron momentum. First the momenta of the lepton and the 'charm' track (reconstructed in the decay-length measurement described above) are summed, with on average a combined momentum of 20 GeV. This is then corrected for the missing neutrino of the semileptonic decay, using a missing-energy technique. The difference between the beam energy and the sum of all visible energy [13] in the hemisphere that contains the lepton is taken as an estimate of the neutrino momentum, with an average value of 9 GeV. This is added to the charged momentum calculated above, and finally a correction is applied to account for the neutral energy of the b decay. Following Monte Carlo studies 68 % of the neutral energy in the jet (on average 9 GeV) is assigned to the b decay, giving the final estimate of the b hadron momentum, p_b. The boost term is then taken as m_b/p_b, where a b hadron mass of 5.3 GeV is assumed. The resolution on the boost term for Monte Carlo b decays is shown in Figure 2 (c). It is parametrized with the sum of two Gaussians with widths (0.13, 0.34) and fractions (0.63, 0.37) respectively. Also shown as a dashed histogram is the distribution obtained if the average b hadron momentum were simply used in the estimation of the boost (which would be equivalent to working in decay length rather than proper time). The resulting distribution reflects the b fragmentation function, and is strongly asymmetric, with a rather poorer resolution than the technique just described.

Following Equation (5), the error on the reconstructed decay time is

$$\sigma(t) = \frac{m_b}{p_b}\,\sigma(d) \oplus \frac{\sigma(m_b/p_b)}{m_b/p_b}\,t\ , \tag{6}$$

i.e. the sum in quadrature of a constant term, from the decay-length resolution, and a term proportional to t from the boost. Expressed in terms of proper-time, the average decay-length resolution for the data corresponds to 0.3 ps. The parametrizations described above are used for the decay-length and boost contributions to the resolution, so the final expression for the resolution function has six Gaussian components, with proper-time dependent widths.

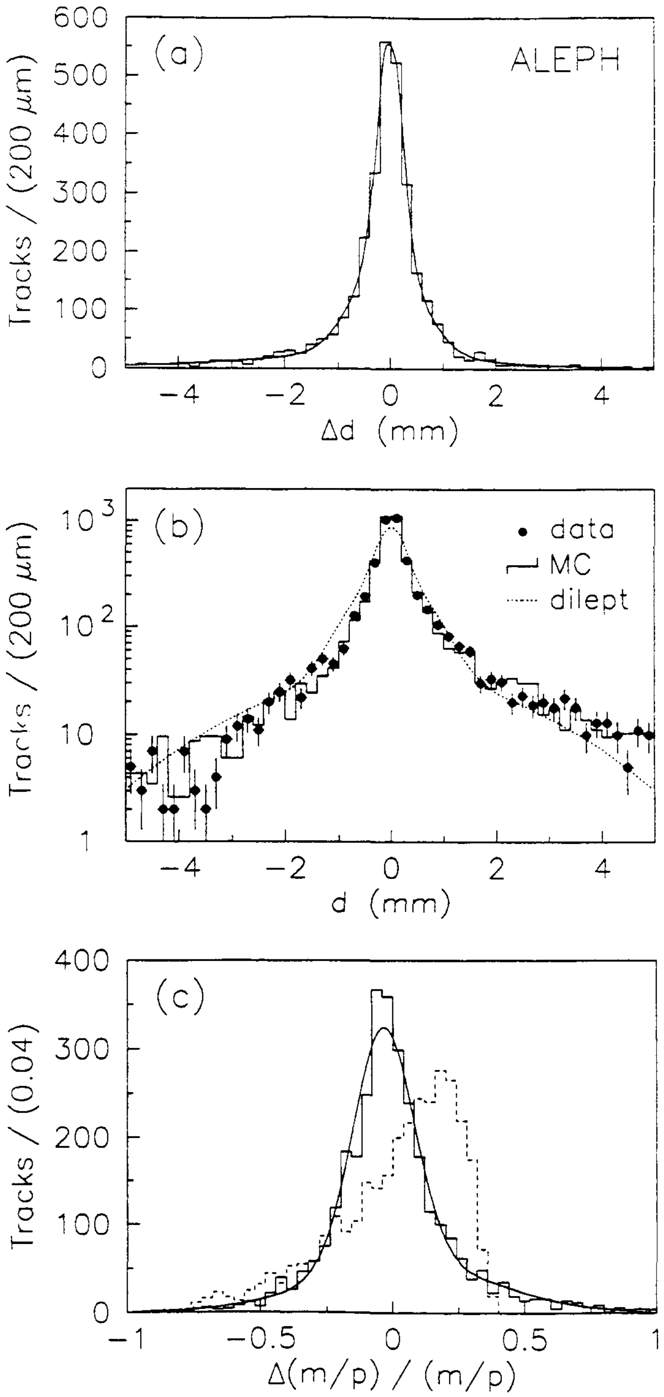

Figure 2: Contributions to the decay-time resolution. (a) Decay-length resolution determined for b decays using Monte Carlo dilepton events; Δ here denotes (reconstructed$-$true) value. (b) Decay-length resolution measured using fake leptons as described in the text; the dotted line shows the Monte Carlo dilepton parametrization from (a). (c) Boost resolution after the b hadron momentum reconstruction has been attempted (with the distribution obtained using only the average b hadron momentum shown as a dashed histogram).

4 Decay-time distributions

The decay-time distributions expected for each of the possible sources of leptons are next determined. For leptons originating from the semileptonic decay of a b hadron (in the absence of mixing) the 'true' decay-time distribution should simply be exponential, with slope given by the lifetime of the parent hadron. The average lifetime of b hadrons is used, denoted τ_b. The reconstructed decay-time distribution that is expected is then a convolution of the exponential distribution with the resolution function determined in the previous section. The resulting normalized probability density is denoted P_b. For B^0 mesons that have mixed, the true distribution follows the form given in Equation (1), where there are two contributions, from B_d^0 and B_s^0 mesons, each with appropriate lifetime (τ_d, τ_s) and oscillation frequency (Δm_d, Δm_s). After convolution with the resolution function, the resulting normalized probability density functions are denoted P_d and P_s. For the small contribution of $b \to \tau \to \ell$ and $b \to J/\psi \to \ell$ decays, the proper-time distributions obtained from Monte Carlo simulation are found to be little different from that of direct b decay, so the same distribution P_b is assumed.

The decay-time distributions also need to be determined for the other sources of leptons, listed in Table 1. For the $b \to c \to \ell$ component, the extra charm decay increases the overall decay length on average, relative to direct $b \to \ell$ decays. This is accounted for by convoluting the underlying distribution assumed for b decays with an extra exponential distribution, which is assigned a lifetime that is left as a free parameter. Fitting to Monte Carlo $b \to c \to \ell$ decays, using the true boost of the b hadron, yields an effective lifetime of (0.15 ± 0.03) ps. Furthermore, the reconstructed momentum is on average underestimated for these decays, due to the more frequent misassignment of tracks. This is accounted for with a second parameter that gives an overall scale factor for the proper-time of $b \to c \to \ell$ decays; it is determined using Monte Carlo events to be 1.22.

The $b \to c \to \ell$ parametrization P_{bc} can be checked using same-side, opposite-sign dilepton events. These are selected as described in Section 2, but requiring that the leptons be in the same jet. They should be predominantly from cascade decays in which both b and c hadrons decay semileptonically. There is also a contribution from $b \to J/\psi \to \ell^+\ell^-$, which is suppressed by requiring that the dilepton invariant mass be less than 3.0 GeV. Roughly half of the remaining leptons should have a decay-time distribution similar to the $b \to c \to \ell$ component of the opposite-side dileptons. Taking into account the small component of misidentified leptons, the expected composition of the decay-time distribution for same-side opposite-sign dileptons is $0.56\, P_b + 0.44\, P_{bc}$. This form is fitted to Monte Carlo events, leaving the scale factor in P_{bc} as a free parameter, and gives a value of 1.17 ± 0.11. The equivalent distribution for the real data is shown in Figure 3 (a), with the result of the fit superimposed: this gives a value of 1.20 ± 0.14. Correcting by the ratio of these results, the final value taken for the scale factor in opposite-side dilepton events is 1.25 ± 0.19.

The prescription described here for the conversion of a $b \to \ell$ decay into a $b \to c \to \ell$ decay allows the consistent treatment of all the b decay subsamples: for B^0 mesons that have mixed, the corresponding cascade contribution is calculated by convoluting Equation (1) with the extra lifetime, and then scaling by the scale factor; the resulting normalized probability densities are denoted P_{dc} and P_{sc} for the B_d^0 and B_s^0 cascade decays, respectively.

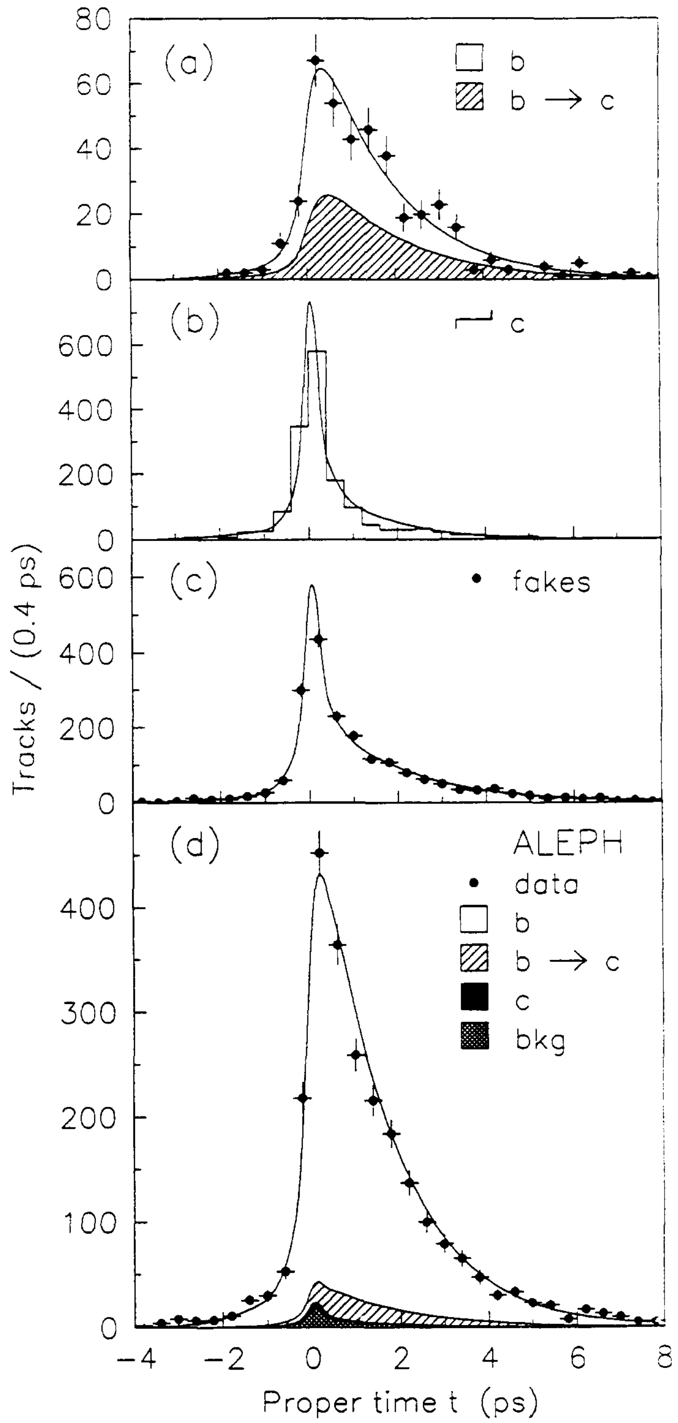

Figure 3: Decay-time distributions, with fits superimposed. (a) Same-side dilepton distribution for real data. (b) Charm decay distribution from Monte Carlo simulation. (c) Fake lepton distribution. (d) Reconstructed decay-time distribution for all of the leptons in the opposite-side dilepton sample, for real data, with the contributions to the fit indicated.

For leptons from charm decay the expected proper-time distribution is taken from Monte Carlo simulation, as shown in Figure 3 (b). For the misidentification background, the expected distribution is determined using the data. The same decay-time reconstruction is used as in the standard analysis, but one of the leptons is replaced with a fake lepton. The resulting proper-time distribution for the fake leptons is shown in Figure 3 (c). Both of these distributions are parametrized using the sum of two exponential components, convoluted with the resolution function, as shown superimposed on the figures. After normalization these parametrizations are taken as the probability density functions P_c and P_{bkg}. For the few decays from other background sources listed in Table 1, any difference from the properties of misidentified leptons is neglected.

With the proper-time distributions for all of the various lepton sources now determined, a fit is made to the complete dilepton sample. The relative contributions of the various sources are taken from the Monte Carlo, as listed in Table 1. If this procedure is applied to the Monte Carlo dilepton sample, and the average b hadron lifetime τ_b is left as a free parameter (with $\tau_d = \tau_s = \tau_b$, as was input to the Monte Carlo generator), the fit gives $\tau_b = (1.27 \pm 0.02)$ ps, consistent with the true value of 1.26 ps for the selected events. However, this differs slightly from the value of 1.30 ps that was input to the simulation; the 3 % bias is a result of the χ^2 cut for the b decay vertex, and is corrected for in the data fits. Applying the fit to the real data gives the result shown in Figure 3 (d), with the contribution to the fit from the different sources indicated. The average b hadron lifetime is measured to be $\tau_b = (1.48 \pm 0.03)$ ps, where the error is statistical only. This agrees with the world average, $\tau_b = (1.49 \pm 0.04)$ ps [6], giving confidence in the calibration of the reconstructed proper time.

5 The like-sign fraction

The true decay-time distribution for B^0 decays, where the B^0 has mixed, has the form given in Equation (1). Thus for a pure sample of B^0 decays, the ratio of the decay-time distribution for mixed events and the distribution for the total sample would be $(1 - \cos(\Delta m t))/2$. If now, instead of using decays which are known to have mixed, the ratio is formed using semileptonic B^0 decays with a like-signed lepton on the other side of the event, the time-dependence stays the same but its amplitude is reduced by mistagging: the probability that the decay is truly that of a mixed B^0 is just $(1 - \chi)$, where χ is the probability that the B^0 on the other side had mixed. Furthermore a fraction χ of the decays will be of unmixed B^0 mesons, with complementary time-dependence to the mixed signal. Thus the expected distribution for the 'like-sign fraction' Q, defined as the ratio of the number of like-sign to total dilepton events as a function of proper-time, is

$$\begin{aligned} Q(t) \equiv \left[\frac{N_{lik}}{N_{lik} + N_{unl}}\right]_t &= (1-\chi)\,\frac{1 - \cos(\Delta m t)}{2} + \chi\,\frac{1 + \cos(\Delta m t)}{2} \\ &= \chi + (1 - 2\chi)\,\frac{1 - \cos(\Delta m t)}{2}\,. \end{aligned} \tag{7}$$

Here N_{lik} and N_{unl} denote the number of like- and unlike-sign events, respectively. This expression must be generalized to include backgrounds and the effect of resolution, but it

Number	Source	Fraction
164	$B^0_d \to \overline{B}^0_d \to \ell$	0.31
120	$B^0_s \to \overline{B}^0_s \to \ell$	0.23
20	$b \to J/\psi \to \ell$	0.04
191	$b \to c \to \ell$	0.37
24	Misidentified	0.05

Table 2: Composition of the wrong-signed lepton candidates (with measured decay time) in the Monte Carlo like-sign dilepton sample.

is clear that $B^0\overline{B}^0$ oscillation should be visible in a plot of the like-sign fraction, as an oscillatory component with frequency Δm.

Apart from mixing, the other causes of mistagging a b decay are $b \to c$ decays, $b \to J/\psi$ decays and misidentified leptons. These processes can lead to 'wrong-signed' leptons, i.e. leptons with a sign opposite to that expected in an unmixed $b \to \ell$ decay. Thus the overall mistagging probability f_w is given by

$$\begin{aligned}(1-f_c)\,f_w \;=\;& [(1-w_b)\overline{\chi} + w_b(1-\overline{\chi})]\; f_b + \\ & [(1-w_{bc})\overline{\chi} + w_{bc}(1-\overline{\chi})]\; f_{bc} + w_{bkg} f_{bkg}\;.\end{aligned} \quad (8)$$

Here f_i ($i = b, bc, c, bkg$) is the fraction of decays in the dilepton sample from the corresponding source of leptons listed in Table 1; w_i is the fraction of the wrong-signed leptons from each source; $\overline{\chi}$ is defined in Equation (4), and the factor $(1-f_c) = f_b + f_{bc} + f_{bkg}$ arises since mistagging only concerns $b\overline{b}$ events. The wrong-signed leptons from direct b decays are due to the $b \to J/\psi$ contribution, and thus w_b is expected to be small; for cascade decays all leptons are wrong-signed, except for those in which the charm quark is produced from the W (i.e. $b \to \overline{c}$ instead of $b \to c$), and thus w_{bc} is close to one. The wrong-sign fraction of misidentified leptons, w_{bkg}, is expected to be close to 0.5.

The mistagging probability can be calculated from the total number of like-sign dileptons, since $N_{lik}/(N_{lik} + N_{unl}) = 2f_w(1-f_w)(1-f_c)$. In the Monte Carlo sample there are 1038 leptons with measured decay time which have a like-signed lepton on the other side of the event, so $f_w = 0.17$. The like-sign dilepton events necessarily include one right-signed and one wrong-signed lepton, and the composition of the wrong-signed leptons is shown in Table 2. For the real data there are 711 leptons with measured decay time which have a like-signed lepton on the other side of the event, also giving a mistagging probability of 0.17.

In the fit described in the next section the values of w_b and w_{bc} are taken from the Monte Carlo simulation, with substantial uncertainty allowed for systematic error studies: $w_b = 0.008 \pm 0.004$ and $w_{bc} = 0.95 \pm 0.03$. The value of w_{bkg} is measured from the data, using the fake lepton analysis described in the previous section: the fraction of events in which the fake lepton has the same sign as the true lepton should be $(1-f_w)\,w_{bkg} + f_w(1-w_{bkg})$. This fraction is measured to be 0.46 ± 0.02 and hence $w_{bkg} = 0.44$.

The like-sign fraction Q for the Monte Carlo dilepton sample is shown in Figure 4 (a), as a function of the reconstructed decay time. The predicted distribution is calculated as the sum of contributions from each possible source of like-sign dileptons, where the contribution from a given source is just the ratio of its expected decay-time distribution to that of the full dilepton sample (shown in Figure 3 (d) for the real data). The Monte Carlo events were generated with $f_d = 0.39$, $f_s = 0.12$, $\Delta m_d = 0.54\,\mathrm{ps}^{-1}$ and $\Delta m_s = 1.85\,\mathrm{ps}^{-1}$. The rise in Q with increasing t due to the B_d^0 contribution is clearly visible, whilst the B_s^0 oscillation adds a small 'wiggle' at short proper-time. The sensitivity to the B_d^0 variables is illustrated in Figure 4 (b), where the distributions that result for different values of Δm_d, τ_d and f_{bc} are shown. As can be seen, varying τ_d acts approximately like a change of amplitude for the oscillation, whilst varying the fraction of the most serious source of background, from $b \to c$ decays, acts like a change in offset; Δm_d changes the frequency of the B_d^0 oscillation as expected. Other parameters to be considered are f_d (which changes the amplitude), τ_b and τ_s (which have little effect on this distribution), and f_s (which, if Δm_s is large, acts like a change in offset). The like-sign fraction for the data is shown in Figure 5 (a); the superimposed fit is described in the following section.

6 B_d^0 oscillation fit

For events with the proper time measured for both leptons, a fit cannot be made to the like-sign fraction distribution to extract the oscillation parameters without double-counting information: although the time-dependent information from the two leptons is independent, the like- or unlike-sign state is a property of the event. Instead, a maximum-likelihood technique is used, with each event contributing to the likelihood according to whether it is like- or unlike-sign, with the decay times on both sides of the event being used in the likelihood calculation. The probability density $F_w(t)$ for a decay at proper time t to be wrong-signed (i.e. resulting in a lepton with opposite sign to that of a $b \to \ell$ decay) is given by a generalization of the mistagging probability of Equation (8):

$$\begin{aligned}(1-f_c)\,F_w(t) &= \left[(1-w_b)\overline{F}_b(t) + w_b\left(P_b(t) - \overline{F}_b(t)\right)\right] f_b + \\ &\quad \left[(1-w_{bc})\overline{F}_{bc}(t) + w_{bc}\left(P_{bc}(t) - \overline{F}_{bc}(t)\right)\right] f_{bc} + w_{bkg} f_{bkg} P_{bkg}(t)\;, \end{aligned} \quad (9)$$

where the probability densities P_i were defined in Section 4; $\overline{F}_b(t) \equiv f_d\chi_d P_d(t) + f_s\chi_s P_s(t)$, and $\overline{F}_{bc}(t) \equiv f_d\chi_d P_{dc}(t) + f_s\chi_s P_{sc}(t)$. The probability density $F_r(t)$ for a b decay to give a right-signed lepton is simply obtained by the substitution $w_i \to (1 - w_i)$. The likelihood contributions for like- and unlike-sign events are then

$$\mathcal{L}_{lik}(t_1,t_2) = (1-f_c)\left[F_r(t_1)F_w(t_2) + F_w(t_1)F_r(t_2)\right]\;, \quad (10)$$

$$\mathcal{L}_{unl}(t_1,t_2) = (1-f_c)\left[F_r(t_1)F_r(t_2) + F_w(t_1)F_w(t_2)\right] + f_c P_c(t_1)P_c(t_2)\;, \quad (11)$$

where t_1 and t_2 are the decay times on the two sides of the event. If only one decay time is measured for the event then the function is integrated over the other time, resulting in $\mathcal{L}_{lik}(t) = (1-f_c)\left[F_r(t)f_w + F_w(t)(1-f_w)\right]$, and similarly for $\mathcal{L}_{unl}(t)$. Here f_w is calculated using Equation (8), with the dependence of $\overline{\chi}$ on Δm_d and Δm_s taken into account. The overall likelihood $\mathcal{L}$ for the event sample is calculated as the product of the likelihood contributions for each event, and $-\log\mathcal{L}$ is minimized in an unbinned fit.

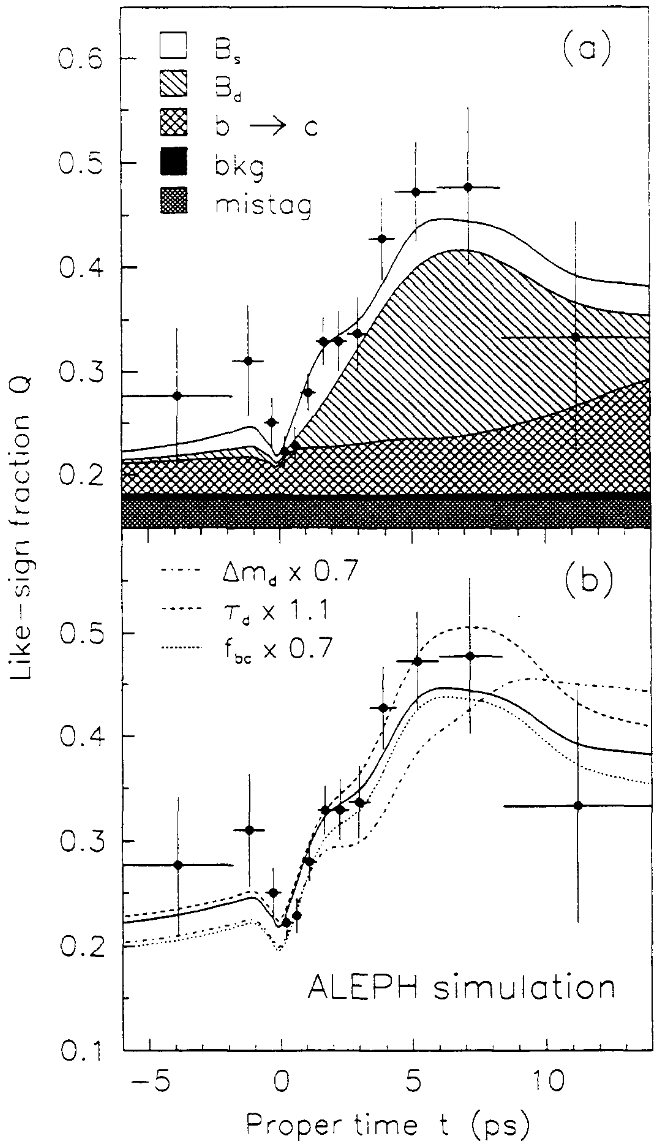

Figure 4: Like-sign fraction for reconstructed Monte Carlo events. (a) Contributions from the various sources of like-sign dileptons are shown superimposed. (b) Sensitivity to the B_d^0 parameters: the solid line shows the nominal prediction; the broken lines show the result of varying parameters as indicated.

Parameter	Fitted value	Constraint
Δm_d	$(0.499\ ^{+0.122}_{-0.107})\,\mathrm{ps}^{-1}$	Free
τ_b	$(1.475 \pm 0.035)\,\mathrm{ps}$	Free
τ_d/τ_b	0.956 ± 0.059	0.993 ± 0.073
f_{bc}	0.066 ± 0.009	0.070 ± 0.010
f_d	0.369 ± 0.029	0.373 ± 0.030
f_s	0.123 ± 0.030	0.150 ± 0.044

Table 3: Result of the oscillation fit for the data, assuming maximal B_s^0 mixing.

As discussed in the previous section, there are at least eight variables upon which the likelihood depends, and given the limited statistics it is necessary to apply constraints. At first, maximal mixing is assumed for the B_s^0, corresponding to a time-independent behaviour (where $B_s^0 \to \ell$ decays are mixed with probability $\chi_s = 0.5$, and have a simple exponential for their underlying decay-time distribution). The B_s^0 lifetime then has little effect, and is fixed to the world average $\tau_s = (1.26\ ^{+0.22}_{-0.17})\,\mathrm{ps}$ [6], where the uncertainty will be accounted for in the systematic error. The fit is performed with Δm_d left free, and also τ_b, as the average b hadron lifetime is an essentially orthogonal variable. Four other parameters, τ_d/τ_b, f_{bc}, f_d and f_s, are allowed to vary in the fit, but they are constrained to their expected values using Gaussian constraints. For the B_d^0 lifetime the world average is used, $\tau_d = (1.48 \pm 0.10)\,\mathrm{ps}$ [6]. For the cascade background fraction the value is taken from the results of a global fit to single lepton and dilepton events [17], which is used to measure the branching ratios of $b \to \ell$ and $b \to c \to \ell$; this gives $f_{bc} = (7.0 \pm 1.0)\%$, where the error includes the model dependence and branching ratio uncertainties.

Analysis of D_s^+ lepton correlations at LEP [18] permits the measurement of the branching ratio product $f_s\,Br(B_s^0 \to D_s^- \ell^+ X)\,Br(D_s^- \to \phi\pi^-) = (4.1 \pm 1.1) \times 10^{-4}$, and studies of inclusive D_s^+ production [19] give $f_s\,Br(B_s^0 \to D_s^- X)\,Br(D_s^- \to \phi\pi^-) = (4.8 \pm 1.0) \times 10^{-3}$. Taking the inclusive semileptonic branching ratio of b hadrons to be $(11.0 \pm 0.5)\%$ [6], $Br(D_s^+ \to \phi\pi^+) = (3.3 \pm 0.7)\%$ [20], and assuming both the fraction of semileptonic and of inclusive B_s^0 decays that give a D_s^- are 0.85 ± 0.15, these results may be used to extract $f_s = 0.15 \pm 0.04$. A similar analysis of $\Lambda\ell$ correlations [19] gives an expected b baryon fraction of 0.11 ± 0.04, and allowing up to 5 % difference in the production rates of B^+ and B_d^0 this implies $f_d = 0.37 \pm 0.03$.

The result of the fit is given in Table 3. The constrained parameters have fitted values that do not differ substantially from those input, although a rather lower value is preferred for the B_s^0 fraction. The value for the average b hadron lifetime agrees well with the single parameter fit performed previously, and the B_d^0 oscillation frequency is measured to be $\Delta m_d = (0.50\ ^{+0.12}_{-0.11})\,\mathrm{ps}^{-1}$. To visualize the quality of the unbinned likelihood fit, the result is projected onto one proper-time dimension, and binned, as shown in Figure 5 (a). The resulting χ^2 is compared to the distribution of χ^2 values obtained for a large number of simulated experiments, and the probability of a worse fit for the data is determined in this way to be 63 %. The result of the fit is compared in Figure 5 (b) with the distribution predicted by a model of time-independent mixing, which is clearly disfavoured. (Note that in this case the

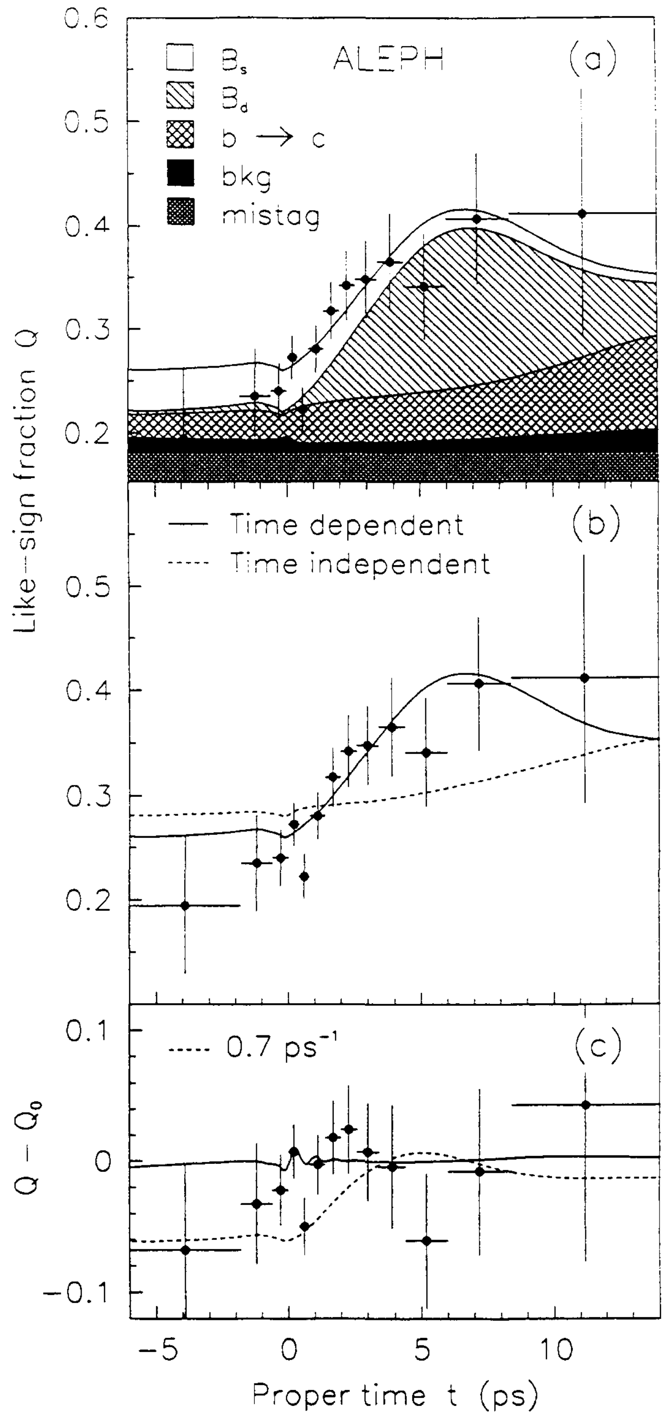

Figure 5: Like-sign fraction for the data. (a) The result of the fit assuming maximal B_s^0 mixing, with the contributions from the various sources of like-sign dileptons indicated. (b) The result of the fit assuming maximal B_s^0 mixing (solid line), compared to a hypothesis of time-independent mixing (dashed line). (c) The difference of the data from the fit in (a), denoted Q_0, with the result of the fit with Δm_s as a free parameter shown as a solid line; the result for a lower value of Δm_s is shown as a dashed line.

Parameter	σ_{sys} (ps^{-1})	
τ_d/τ_b	+0.032	− 0.028
f_{bc}	+0.042	− 0.043
f_d	+0.037	− 0.026
f_s	+0.079	− 0.068
Subtotal	+0.100	− 0.086
τ_s	+0.010	− 0.008
f_c	+0.002	− 0.002
f_{bkg}	+0.021	− 0.019
Resolution	+0.016	− 0.016
Boost	+0.018	− 0.018
Δm_s	+0.028	− 0.000
Other	+0.021	− 0.021
Total	+0.111	− 0.094

Table 4: Contributions to the systematic error on Δm_d.

residual time dependence of the like-sign fraction is due to the background, principally from the cascade decays.) Performing the fit with such a model leads to an increase in negative log-likelihood of 8.0, which corresponds to the time-independent hypothesis being ruled out at greater than 99 % confidence level.

7 Systematic errors

The statistical error on the measurement of Δm_d is evaluated by fixing the parameters in the fit except Δm_d and τ_b to their fitted values (listed in Table 3) and then refitting. The result is $\Delta m_d = (0.50\ ^{+0.07}_{-0.06})\,\mathrm{ps}^{-1}$, where the contribution to the error from the uncertainty on the fitted value of τ_b is only $\pm 0.004\,\mathrm{ps}^{-1}$. The difference in quadrature between this error on Δm_d and that from the fit where the other parameters were allowed to vary, $^{+0.10}_{-0.09}\,\mathrm{ps}^{-1}$, is taken as the systematic error resulting from the uncertainty on those parameters. To estimate the individual contributions to this systematic error, each parameter was allowed to float in turn, and the resulting contribution to the error on Δm_d (calculated in quadrature) is listed in Table 4. The sum in quadrature of these individual contributions is slightly greater than the value given by allowing them all to float simultaneously (labelled 'subtotal' in the table) due to correlations between the parameters. The effect of the uncertainty on these parameters is the dominant source of systematic error.

The other contributions in the table are calculated by varying the parameters concerned within their uncertainties, and checking the effect on the fitted value of Δm_d. For the B^0_s lifetime the uncertainty on the world average value is taken, whilst for the charm and misidentification background fractions a 50 % relative error is assumed. For the decay-length resolution the contribution is calculated by varying the scale factor by 10 % and varying the

p_T (GeV)	N_{ev}	Δm_d (ps^{-1})
1.00	3005	$0.60 \pm 0.09 \pm 0.16$
1.25	1863	$0.50 \pm 0.07 \pm 0.11$
1.50	1126	$0.54 \pm 0.08 \pm 0.11$
1.75	656	$0.50 \pm 0.09 \pm 0.11$
2.00	353	$0.54 \pm 0.13 \pm 0.12$

Table 5: Dependence on the lepton p_T cut of the result for the B_d^0 oscillation frequency; N_{ev} is the number of dilepton events.

offset by 100 %. For the boost, the contribution to the systematic error is taken as the uncertainty on the proper-time scale, 3.6 %, evaluated by comparing the measured b lifetime with its world average value. For Δm_s the contribution is taken as the difference between the results for maximal B_s^0 mixing and for $\Delta m_s = 3\,\mathrm{ps}^{-1}$ (corresponding to the lower limit on $\Delta m_s/\Delta m_d$ from the Standard Model, discussed in Section 1). Finally the contribution in Table 4 labelled 'other' gives the sum in quadrature of the effects of all other variables that have been investigated; this includes w_b, w_{bc}, w_{bkg}, and the parametrizations of P_{bc}, P_c and P_{bkg}. All of the contributions are combined in quadrature to give the final result $\Delta m_d = (0.50\ ^{+0.07}_{-0.06}\ ^{+0.11}_{-0.10})\,\mathrm{ps}^{-1}$, where the first error is statistical and the second systematic.

Various checks of the result have been performed. Firstly, the same analysis has been applied to the Monte Carlo sample, giving the result $\Delta m_d = (0.55 \pm 0.05)\,\mathrm{ps}^{-1}$, in good agreement with the input value of $0.54\,\mathrm{ps}^{-1}$. The analysis has been repeated requiring that the leptons for which the decay time is measured be only muons, only electrons, or both an electron and a muon, with the compatible results $(0.47 \pm 0.09)\,\mathrm{ps}^{-1}$, $(0.65 \pm 0.17)\,\mathrm{ps}^{-1}$ and $(0.38 \pm 0.12)\,\mathrm{ps}^{-1}$ respectively (statistical errors). Selecting events for which there is a proper-time measurement on both sides of the event, or only one, the results are $(0.46 \pm 0.08)\,\mathrm{ps}^{-1}$ and $(0.51 \pm 0.11)\,\mathrm{ps}^{-1}$, again in good agreement.

The full analysis has been repeated for different values of the lepton p_T cut. It is found that the underlying proper-time distributions are largely independent of p_T, whilst the resolution improves slightly with increasing p_T. Furthermore, the composition of the sample changes, with reduced background at high p_T. The results for the oscillation frequency are given in Table 5. The measurement of Δm_d is stable with p_T, with the minimum total error at the cut $p_T > 1.25\,\mathrm{GeV}$ that has been used throughout.

8 B_s^0 oscillation limit

The frequency of oscillation for the B_s^0 is next allowed to vary in the fit, as a third free parameter. The dependence of the likelihood on Δm_d and Δm_s is shown in Figure 6 (a): the favoured value for Δm_d as a function of Δm_s (indicated by the dot-dashed line in the figure) is determined by the time-integrated information in the fit, corresponding to constant $\overline{\chi}$. Discrimination amongst the points on this line is provided by the time-dependent information, with maximum likelihood occurring for $\Delta m_s = 9.0\,\mathrm{ps}^{-1}$; for this value of Δm_s

the other parameters in the fit do not vary significantly from those listed in Table 3.

The effect of B_s^0 oscillation is illustrated in Figure 5 (c), where the like-sign distribution for the data is shown after subtraction of the function $Q_0(t)$ given by the fit with maximal B_s^0 mixing. The result of the fit with Δm_s as a free parameter is shown superimposed as a solid line; the distribution that would result for a lower value of Δm_s is also shown.

The dependence of the likelihood on Δm_s, for Δm_d held at its fitted value, is shown by the solid line in Figure 6 (b), where the difference in $-\log \mathcal{L}$ is given relative to the result obtained assuming maximal B_s^0 mixing. Refitting for Δm_d at each point leads to the dot-dashed line in the figure, which corresponds to the likelihood profile along the dot-dashed line in Figure 6 (a). Low values for Δm_s are increasingly disfavoured, until $\Delta m_s = \Delta m_d$. This point is excluded at greater than 99 % confidence level, since the oscillation frequency of $0.74\,\mathrm{ps}^{-1}$ required by the time-integrated information is incompatible with the time-dependence, as can be seen in Figure 5 (c). Further decrease in Δm_s leads to less disfavoured values, as the B_d^0 and B_s^0 exchange roles in the fit; the situation is not entirely symmetric, however, since the assumed production rates of the mesons differ, and the point $\Delta m_s = 0\,\mathrm{ps}^{-1}$ is still excluded at greater than 95 % confidence level. Such low values of Δm_s have anyway been ruled out by previous time-integrated measurements, as discussed in Section 1.

The error on the fitted value of Δm_s is unconstrained on the upper side; the 95 % confidence level would nominally be given by the value of Δm_s for which the negative log-likelihood increases by 1.92, but due to the non-parabolic nature of the log-likelihood the lower limit has instead been derived with the help of Monte Carlo simulation. The events in the standard sample may be 'remixed' to any chosen value of Δm_s, by checking whether each lepton in the sample has come from a B_s^0 decay: if this is the case, and the B_s^0 mixed before decaying, then the like- or unlike-sign state of the event is reversed. The probability that the B_s^0 would have mixed is then calculated for the new value of Δm_s (using the true proper-time of the decay), and the like- or unlike-sign state is kept unchanged or reversed accordingly, thus simulating the new mixing. This procedure is repeated to produce many samples of equal statistics to the data at each input oscillation frequency. For input values of Δm_s less than about $2\,\mathrm{ps}^{-1}$ a clear minimum is seen in $-\log \mathcal{L}$ at the correct Δm_s; for higher input values this is no longer the case, due to the limited statistics.

The input value of Δm_s was scanned from 0 to $12\,\mathrm{ps}^{-1}$ in $0.1\,\mathrm{ps}^{-1}$ steps, and at each value 1000 samples of remixed Monte Carlo events were generated. For each of these samples the difference in log-likelihood relative to an assumption of maximal B_s^0 mixing, denoted L, was calculated using a value of Δm_s equal to the input value. The limit L_0 was then determined for which 950 out of the 1000 samples satisfy $L < L_0$: this corresponds to the 95 % confidence level that, for a given true value of Δm_s, the value of L would be less than L_0 when calculated at that Δm_s. The resulting curve is superimposed on Figure 6 (b) as the lower dotted line.

The effect of systematic biases has been studied by varying all the parameters in the likelihood calculation, as described in the previous section for the Δm_d fit, and then repeating the analysis. The distribution of L_0 that gives the lowest limit following from these studies is shown superimposed on Figure 6 (b) as the upper dotted line. The final limit is taken as the intersection of this curve with the L distribution for the data, and is $\Delta m_s > 1.8\,\mathrm{ps}^{-1}$ (95 % CL). The effect of a difference in width $\Delta\Gamma$ between the two B_s^0 mass eigenstates has

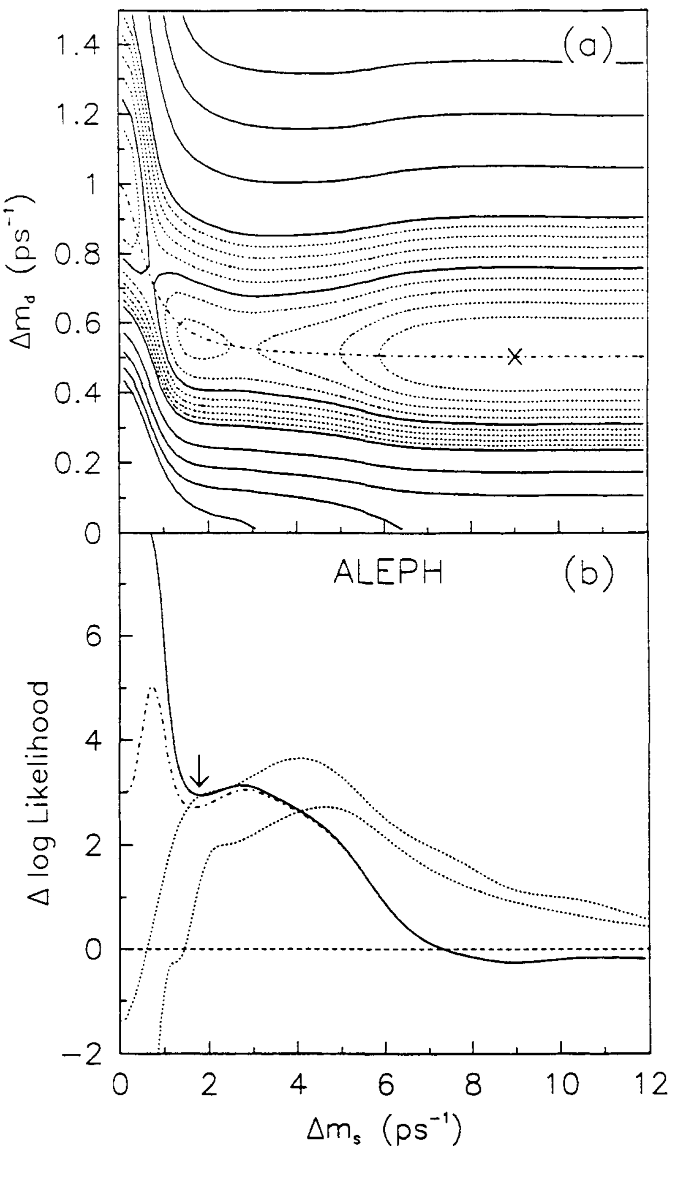

Figure 6: Setting a limit for Δm_s. (a) Contour plot of the negative log-likelihood as a function of Δm_d and Δm_s; the cross indicates the minimum, the solid contours are spaced by 5 units in $-\log\mathcal{L}$, and the dotted contours are spaced by one unit; the dot-dashed line shows the locus of minima for Δm_d as a function of Δm_s. (b) The difference in $-\log\mathcal{L}$ (relative to the value for maximal B_s^0 mixing) as a function of Δm_s, for fixed Δm_d (solid line), and refitted Δm_d (dot-dashed line); the 95 % confidence contours described in the text are shown as dotted lines, and the arrow indicates the final limit.

been investigated and is negligible for $\Delta\Gamma/2\Gamma < 0.3$.

An independent analysis has been performed, for which the main differences were that a higher p_T cut was applied to the leptons, the average b hadron momentum was used in the calculation of the boost, and a binned fit was performed. The results obtained for both Δm_d and Δm_s are consistent with those reported here.

9 Conclusions

$B^0\overline{B}^0$ oscillation has been studied using the vertex structure of events containing two leptons, on opposite sides of the event, in a sample of 977,000 hadronic Z decays. An analysis of the decay-time distribution of 2479 selected leptons with $p_T > 1.25\,\mathrm{GeV}$ has provided clear evidence for the time-dependent nature of $B_d^0\overline{B}_d^0$ mixing. The possibility of time-independent $B_d^0\overline{B}_d^0$ mixing is excluded at the 99 % confidence level. This confirms the previous observation of the effect by the ALEPH collaboration [21], from an analysis of D^{*+} lepton correlations. The value measured for the oscillation frequency, $(0.50\ ^{+0.07}_{-0.06}\ ^{+0.11}_{-0.10})\,\mathrm{ps}^{-1}$, corresponds to a mass difference for the B_d^0 mass eigenstates of

$$\Delta m_d = (3.29\ ^{+0.45}_{-0.42}\ ^{+0.73}_{-0.62}) \times 10^{-4}\,\mathrm{eV}/c^2\ . \tag{12}$$

This is in good agreement with the other direct measurement of this quantity, from the $D^{*+}\ell$ analysis, of $(3.44\ ^{+0.65}_{-0.70}\ ^{+0.26}_{-0.20}) \times 10^{-4}\,\mathrm{eV}/c^2$. The only significant correlation between these two measurements is through the influence of the B_d^0 lifetime, amounting to a common systematic error of $\pm 0.20 \times 10^{-4}\,\mathrm{eV}/c^2$, and they may be averaged to give $\Delta m_d = (3.4 \pm 0.5) \times 10^{-4}\,\mathrm{eV}/c^2$. Assuming the world average for the B_d^0 lifetime this corresponds to $(\Delta m/\Gamma)_d = 0.76 \pm 0.12$, where the uncertainty in the lifetime has been included. This is in good agreement with the time-integrated results of experiments at the $\Upsilon(4S)$ [5], $(\Delta m/\Gamma)_d = 0.68 \pm 0.08$.

Searching for a second frequency component in the decay-time distribution allows a lower limit of $1.8\,\mathrm{ps}^{-1}$ to be set on the oscillation frequency for the B_s^0, or equivalently

$$\Delta m_s > 12 \times 10^{-4}\,\mathrm{eV}/c^2\ (95\,\%\ \mathrm{CL})\ . \tag{13}$$

Assuming the world average for the B_s^0 lifetime of $(1.26\ ^{+0.22}_{-0.17})\,\mathrm{ps}$ this corresponds to $(\Delta m/\Gamma)_s > 2.0$, which improves on the previous limit, from an average of time-integrated measurements, of $(\Delta m/\Gamma)_s > 0.9$. The results for the two mass differences can be combined to give $\Delta m_s/\Delta m_d > 3.2$, which remains lower than the Standard Model prediction $\Delta m_s/\Delta m_d > 8$. Following Equation (3) the result can be converted into a limit on the Kobayashi-Maskawa matrix elements, $|V_{ts}/V_{td}| > 1.6$.

Acknowledgements

It is a pleasure to thank our colleagues in the accelerator divisions of CERN for the excellent performance of LEP. Thanks are also due to the technical personnel of the collaborating institutions for their support in constructing and maintaining the ALEPH experiment. Those of us from non-member states thank CERN for its hospitality.

References

[1] E. Paschos and U. Türke, Phys. Rep. **178** (1989) 145.

[2] A. Ali, Proc. of XXVI Int. Conf. on HEP, Dallas (1992) Vol. I 484.

[3] K. Hikasa *et al.* (Particle Data Group), Phys. Rev. D **45** (1992) 1.

[4] J. Bartelt *et al.* (CLEO Collab.), CLNS 93/1240, submitted to Phys. Rev. Lett.

[5] J. Bartelt *et al.* (CLEO Collab.), Phys. Rev. Lett. **71** (1993) 1680;
H. Albrecht *et al.* (ARGUS Collab.), Z. Phys. C **55** (1992) 357.

[6] M. Danilov, to appear in Proc. of EPS Conf. on HEP, Marseille (1993).

[7] C. Albajar *et al.* (UA1 Collab.), Phys. Lett. B **262** (1991) 171;
F. Abe *et al.* (CDF Collab.), Phys. Rev. Lett. **67** (1991) 3351;
P. Acton *et al.* (OPAL Collab.), Phys. Lett. B **276** (1992) 379;
B. Adeva *et al.* (L3 Collab.), Phys. Lett. B **288** (1992) 395;
P. Abreu *et al.* (DELPHI Collab.), Phys. Lett. B **301** (1993) 145.

[8] D. Decamp *et al.* (ALEPH Collab.), Phys. Lett. B **258** (1991) 236.

[9] D. Decamp *et al.* (ALEPH Collab.), Nucl. Instr. Methods A **294** (1990) 121.

[10] G. Batignani *et al.*, Proc. of IEEE Nucl. Science Symp., Santa Fe (1991) 438.

[11] D. Decamp *et al.* (ALEPH Collab.), Z. Phys. C **53** (1992) 1.

[12] D. Decamp *et al.* (ALEPH Collab.), Phys. Lett. B **263** (1991) 325;
D. Buskulic *et al.* (ALEPH Collab.), Heavy quark tagging with leptons in the ALEPH detector, in preparation.

[13] D. Decamp *et al.* (ALEPH Collab.), Phys. Lett. B **246** (1990) 306.

[14] S. Bethke *et al.* (JADE Collab.), Phys. Lett. B **213** (1988) 235.

[15] T. Sjöstrand and M. Bengtsson, Computer Phys. Commun. **43** (1987) 367.

[16] J. Körner and G. Schuler, Z. Phys. C **38** (1988) 511.

[17] D. Buskulic *et al.* (ALEPH Collab.), Heavy flavour production and decay with prompt leptons in the ALEPH detector, in preparation.

[18] D. Buskulic *et al.* (ALEPH Collab.), Phys. Lett. B **294** (1992) 145;
P. Acton *et al.* (OPAL Collab.), Phys. Lett. B **295** (1992) 357.

[19] F. Pierre, to appear in Proc. of V Int. Symp. on Heavy Flav. Phys., Montreal (1993).

[20] P. Burchat, to appear in Proc. of V Int. Symp. on Heavy Flav. Phys., Montreal (1993).

[21] D. Buskulic *et al.* (ALEPH Collab.), Phys. Lett. B **313** (1993) 498.